Nonlinear plasma instability effects for subharmonic and harmonic forcing oscillations

1972 J. Phys. A: Gen. Phys. 5 152

(http://iopscience.iop.org/0022-3689/5/1/020)

J. Phys. A: Gen. Phys., Vol. 5, January 1972. Printed in Great Britain

Nonlinear plasma instability effects for subharmonic and harmonic forcing oscillations

B E KEEN and W H W FLETCHER

UKAEA Research Group, Culham Laboratory, Abingdon, Berks, UK

MS received 17 June 1971

Abstract. Results are presented which show that a marginal ion sound instability in a plasma behaves in a manner similar to that predicted by a Van der Pol type of nonlinear equation, including anharmonic terms. Experiments have been performed in which the system is subjected to an external driving force at the fundamental frequency ω_0, and the subharmonic frequencies, which shows that the instability exhibits characteristics similar to the classical nonlinear phenomena of 'jumps' including the associated hysteresis effect. When the system is driven by a forcing oscillation at the harmonic frequencies $2\omega_0$ or $3\omega_0$, the instability behaves differently from linear forced resonance, and exhibits a behaviour similar to a parametric oscillator. A theory developed to describe this ion sound instability under these various conditions, is compared with the experimental results, and good agreement is obtained.

1. Introduction

Essentially, a plasma is a nonlinear medium. In the case, when the amplitudes of any selfexcited oscillations or perturbations in a plasma are small, a linear theory may be applied to describe the propagation characteristics and dispersion relationship in this medium. In the past, this procedure has been generally adopted in comparing the results obtained on selfexcited oscillations or instabilities present in a plasma with theoretical predictions, even when the instability amplitude is large. In a number of cases, considerable success has been achieved (eg Hendel *et al* 1968). However, in order to explain, the amplitude characteristics of these various kinds of instabilities and how the amplitude saturates at a finite level, rather than growing to infinite proportions, a nonlinear theory is required. This has led to much recent interest in the possible nonlinear mechanisms which cause this amplitude saturation, and a number of possibilities have been suggested. These include anharmonic effects (Hsuan 1968), mode–mode coupling (Stix 1969) and wave–particle scattering (Dupree 1968). In particular, the mode–mode coupling approach appears to give rise to the plasma instability behaving as a classical Van der Pol (1922) oscillator.

In § 2, this paper develops a theory starting from the two-fluid equations of motion. A nonlinear equation of the Van der Pol type (including anharmonic terms) can be obtained to describe the temporal variation of density perturbations of the ion sound instability. Further, it has been shown that when this system is in its marginal state and is subjected to external driving oscillation at a frequency ω, forced resonance oscillations are observed at the instability frequency ω_0 which are of two types. The two types depend upon the frequency of the driving oscillations ω and are observed when (i)

subharmonic driving oscillations $\omega \simeq \omega_0/m$ ($m = 1, 2, 3, \ldots$) and (ii) harmonic driving oscillations $\omega \simeq m\omega_0$ ($m = 2, 3, \ldots$) are employed.

Section 3 continues to describe the apparatus, the nature of the instability in the apparatus, and the method employed to apply externally derived oscillations in the plasma. In § 4, the results obtained in the two regimes, (i) for subharmonic drives and (ii) for harmonic driving frequencies, are presented. Finally, § 5 compares these results with the theory developed, and suggests how this technique can be used to obtain information on the nonlinear mechanisms in a plasma, and the nonlinear parameters relating to a particular instability.

2. Theory

The plasma stability was investigated by using the 'two-fluid' model, in cartesian geometry, to describe the motion of the electrons and ions separately. The electron equation of motion is given by

$$m\frac{\mathrm{d}\boldsymbol{v}_e}{\mathrm{d}t} = e\nabla\phi - \frac{e}{c}\boldsymbol{v}_e \times \boldsymbol{B}_0 + \frac{T_e}{n}\nabla n \tag{1}$$

where $\boldsymbol{v}_e$ is the electron velocity, T_e the electron temperature, n the plasma density and B_0 the axial magnetic field, which is taken in the z direction.

As the instability of interest in this situation is an $m = 0$ ion sound wave, only spatial variations of the form $\exp(ik_z z)$ need be considered, when k_z is the axial wavenumber associated with this wave. The density n is taken of the form $n = n_0 + n_1$, where n_0 is a steady state average value, and n_1 is an oscillatory value which is a time varying function of z. The potential ϕ is taken with zero steady state value, and a finite oscillatory value ϕ_1. In the low frequency approximation, electron inertia effects may be neglected, and the z component of equation (1) reduces to

$$\frac{n_1}{n} = \frac{e\phi_1}{T_e}. \tag{2}$$

In the ion equation of motion, inertia effects are important, and this equation is given by

$$M\frac{\mathrm{d}\boldsymbol{v}_i}{\mathrm{d}t} + Mv\boldsymbol{v}_i = -e\nabla\phi + \frac{e}{c}\boldsymbol{v}_i \times \boldsymbol{B}_0 \tag{3}$$

where v is the ion neutral collision frequency, and $\boldsymbol{v}_i$ the ion velocity. In this case, the nonisothermal situation has been considered in which $T_i \ll T_e$, and so the pressure gradient term has been ignored.

The ion equation of continuity is

$$\frac{\partial n}{\partial t} + \nabla \cdot (n\boldsymbol{v}_i) = S_i(n, T_e, \boldsymbol{E}). \tag{4}$$

Here S_i is an ion source term which can be caused by the presence of large amplitude fluctuations in the plasma creating plasma locally by electron heating effects, local ionization, etc. Consequently this source S_i is a function of local density n, electron temperature T_e and local electric field $\boldsymbol{E}$. It has been shown previously (Keen and

Fletcher 1969, 1970) from thermodynamic arguments (Hsuan 1968) that this source term is given by an expression of the form

$$S_i = \alpha n_1 - \beta n_1^2 - \gamma n_1^3 - \dots \tag{5}$$

where $\omega_0 = k_z c_s \gg \alpha, \beta n_1$, and γn_1^2, $c_s = (T_e/M)^{1/2}$ is the ion sound velocity and ω_0 is the ion sound instability frequency. Strictly, there should be a source term in the momentum equation but under the condition $\alpha \ll \omega_0$, it can be neglected.

By eliminating v_i, v_e and ϕ_1 between equations (2), (3), (4) and (5), a differential equation for the time varying portion of the density is obtained, namely

$$\frac{d^2 n_1}{dt^2} + \frac{dn_1}{dt}\{(\nu - \alpha) + 2\beta n_1 + 3\gamma n_1^2\} + \omega_0^2 n_1 + \beta \nu n_1^2 + \gamma \nu n_1^3 = 0. \tag{6}$$

It can be shown (Van der Pol 1922) that an equation of this type has a selfoscillatory solution when $(\nu - \alpha) < 0$. In this case, the initial linear growth rate is $(\alpha - \nu)/2$, and γ is a nonlinear saturation coefficient which limits the steady state selfexcited oscillation amplitude at frequency ω_0 to a value $\{4(\alpha - \nu)/3\gamma\}^{1/2}$.

Under the condition that $(\nu - \alpha) > 0$, the instability is damped and no selfexcited oscillation occurs in the system. This is the situation which is considered in this paper. However, when the system is subjected to an external forcing oscillation of frequency ω (not necessarily equal to ω_0) the oscillation at ω_0 may be made to reappear. Consider the case in which the system is subject to a driving force of the form $A \sin \omega t$, then the temporal variation of density is given by

$$\frac{d^2 n_1}{dt^2} + \frac{dn_1}{dt}\{(\nu - \alpha) + 2\beta n_1 + 3\gamma n_1^2\} + \omega_0^2 n_1 = \omega^2 A \sin \omega t - \nu\beta n_1^2 - \nu\gamma n_1^3. \tag{7}$$

2.1. Forcing oscillations near the fundamental or its subharmonics

Consider the case when $(\nu - \alpha) = k > 0$, and that the forcing oscillation is at a frequency ω close to ω_0 ($\omega = \omega_0 + \Delta\omega$, $\Delta\omega \ll \omega_0$). Then, this equation reduces to a standard anharmonic forced resonance type of equation (Minorsky 1962) which can be written as

$$\frac{d^2 n_1}{dt^2} + \omega_0^2 n_1 = f\left(n_1, \frac{dn_1}{dt}\right) + \omega_0^2 A \sin(\omega_0 + \Delta\omega)t$$

where

$$f\left(n_1, \frac{dn_1}{dt}\right) = -\frac{dn_1}{dt}(k + 2\beta n_1 + 3\gamma n_1^2) - \nu\beta n_1^2 - \nu\gamma n_1^3. \tag{8}$$

If a trial solution of the form $n_1 = b \cos(\omega t + \psi)$ is adopted where ψ is a phase angle and $\omega = (\omega_0 + \Delta\omega)$ then upon substitution into equation (8), a cubic equation in b^2 is obtained, correct to second order. Under the condition that $k \gg \gamma b^2$, this equation becomes

$$b^2\left\{\left(2\Delta\omega - \frac{3\nu\gamma b^2}{4\omega_0}\right)^2 + k^2\right\} = \omega_0^2 A^2. \tag{9}$$

The real roots of this cubic equation give the amplitude b of the forced oscillations as ω is varied around ω_0. When the driving amplitude A is small, b is fairly small, and the second term in the bracket on the left hand side of equation (9) may be neglected. This

equation reduces to a standard symmetrical resonance curve, as shown in figure 1(*a*), with a maximum amplitude at $\omega = \omega_0$. As A increases the curve changes its shape, but retains its single maximum which moves to positive $\Delta\omega$, as in figure 1(*b*). When A reaches a certain value A_m, the nature of the curve changes. At this value equation (9) has three real roots for certain values of $\Delta\omega$, corresponding to those values in the region BCDE, in figure 1(*c*). The limits of this range are determined by $db/d(\Delta\omega) = \infty$, which

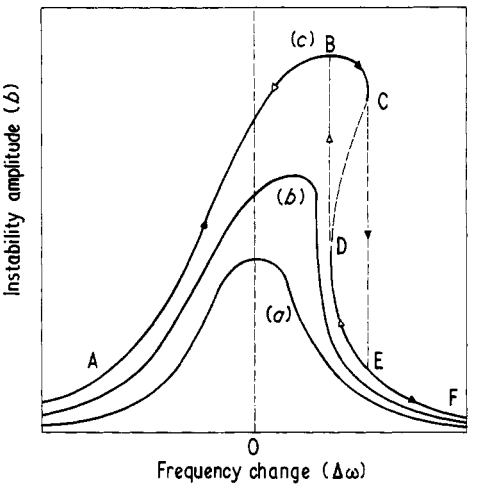

Figure 1. Theoretical instability amplitude as a function of frequency near ω_0, for increasing drive amplitude. See text for (*a*), (*b*) and (*c*).

holds at the points C and D. It has been shown (Minorsky 1962), that the dashed portion of figure 1(*c*) corresponds to an unstable region, and any small perturbation of the oscillator causes the system to 'jump' from the state C to E, or D to B. Consequently, if the frequency is gradually increased from A the path ABC → EF is followed, and if the frequency is decreased starting from F, the path FED → BA is followed. Hence, in this case, the system shows an 'hysteresis' effect. The points C and D are given by $db/d(\Delta\omega) = \infty$ which reduces to

$$4(\Delta\omega)^2 - \frac{6\nu\gamma\Delta\omega b^2}{\omega_0} + \frac{27\nu^2\gamma^2 b^4}{16\omega_0^2} + k^2 = 0. \tag{10}$$

The maximum amplitude b_m is reached at that value given by $db/d(\Delta\omega) = 0$. This is when $3\nu\gamma b_m^2 = 8\omega_0\Delta\omega$, and from equation (9) gives

$$b_m = \frac{\omega_0 A}{k}. \tag{11}$$

Similarly, if the subharmonic drive proportional to $B \sin \frac{1}{2}(\omega_0 + \Delta\omega)t$ is employed, an equation similar to equation (9) is obtained. In this case, A is replaced by $8\beta B^2/9\omega_0^2$, and the maximum amplitude now occurs at

$$b_m = \frac{8\beta B^2}{9k\omega_0}. \tag{12}$$

In the same way, effects should occur at the fundamental frequency ω_0 for forcing

oscillations at ω_0/m, where $m = 2, 3, 4, 5, \ldots$, etc, but in these cases the expansion of the source term S_i given by equation (5) must be taken to the term in n_1^m.

2.2. Forcing oscillations near the second harmonic ($\omega \simeq 2\omega_0$)

If the substitutions $\omega t = \tau$, and $n_1 = \omega_0 x/\beta$ are made in equation (7), the following reduced equation is obtained

$$\frac{d^2x}{d\tau^2}+\frac{dx}{d\tau}\left(\frac{k}{\omega_0}+2x+\frac{3\gamma\omega_0}{\beta^2}x^2\right)+x = \frac{BA}{\omega_0}\sin 2\tau-\frac{\nu}{\omega_0}x^2-\frac{\nu\gamma}{\beta^2}x^3+\frac{2\Delta\omega}{\omega_0}x. \quad (13)$$

This equation can be put in the form

$$\frac{d^2x}{d\tau^2}+x = \lambda\sin 2\tau+F\left(x,\frac{dx}{d\tau}\right) \quad (14)$$

where $F(x, dx/d\tau)$ is a small nonlinear term which produces a small perturbation on the harmonic solution, and is given by

$$F\left(x,\frac{dx}{d\tau}\right) = gx-A_1x^2-A_2x^3-(k_1+2x+A_3x^2)\frac{dx}{d\tau} \quad (15)$$

where A_1, A_2, A_3, k_1 and g may be seen by comparing equations (15) and (14). This type of equation can be solved (Mandelstam and Papalexi 1932) by adopting a trial solution of the form

$$\begin{aligned} x &= a_2\sin\tau-b_2\cos\tau-\frac{\lambda}{3}\sin 2\tau \\ &= X\sin(\tau-\psi)-\frac{\lambda}{3}\sin 2\tau \end{aligned} \quad (16)$$

where ψ is a phase angle and X is the amplitude of the oscillation produced at frequency ω_0.

By substitution of this trial form of solution into equation (14), the following relationships relating a_2 and b_2 are obtained:

$$\begin{aligned} a_2\left\{k+\frac{\lambda A_1}{3}+\frac{A_3}{4}\left(X^2+\frac{2\lambda^2}{9}\right)\right\} &= b_2\left\{\frac{3A_2}{4}\left(X^2+\frac{2\lambda^2}{9}\right)-\frac{\lambda_0}{3}-g\right\} \\ b_2\left\{k+\frac{\lambda A_1}{3}+\frac{A_3}{4}\left(X^2+\frac{2\lambda^2}{9}\right)\right\} &= -a_2\left\{\frac{\lambda}{3}-g+\frac{3A_2}{4}\left(X^2+\frac{2\lambda^2}{9}\right)\right\}. \end{aligned} \quad (17)$$

If $\{X^2+(2\lambda^2/9)\} = Y^2$, an equation quadratic in Y^2 can be obtained

$$\begin{aligned} &\frac{Y^4(A_3^2+9A_2^2)}{16}+Y^2\left\{\frac{A_3}{2}\left(k+\frac{A_1\lambda}{3}\right)-\frac{3A_2g}{2}\right\} \\ &\quad+\left\{g^2+\frac{9A_2^2}{16}+\left(k+\frac{A_1\lambda}{3}\right)^2-\frac{\lambda^2}{9}\right\} = 0. \end{aligned} \quad (18)$$

This equation can be put in the form

$$Y^4+Y^2G(g,\lambda)+H(g,\lambda) = 0 \quad (19)$$

where the variables $g(\Delta\omega)$ and $\lambda(A)$ are related to the shift of the driving frequency $\Delta\omega$ from exact second harmonic ($2\omega_0$) and the driving amplitude A.

A solution for the amplitude X at the fundamental frequency is

$$X^2 = -\frac{2\lambda^2}{9} - \frac{1}{2}G(g, \lambda) + \frac{1}{2}\{G^2(g, \lambda) - 4H(g, \lambda)\}^{1/2}. \tag{20}$$

The principal solution corresponds to real values of X, that is, $X^2 > 0$. Since the term $-2\lambda^2/9$ is always negative, the sum of other terms on the right hand side must be positive and greater than $2\lambda^2/9$ to fulfil this condition. Mandelstam and Papalexi (1932) have shown that there is a minimum value of $\lambda(A)$ required for oscillation to set in, and there is an upper limit for $\lambda(A)$ as well above which oscillation will not occur. They have considered the stability of the situation and find that for exact resonance ($\omega = 2\omega_0$), when $\Delta\omega = 0 = g$, that a relationship between the amplitude X and the drive amplitude $A(\propto\lambda)$ as shown in figure 2, is obtained. It is apparent that oscillations at ω_0 only occur

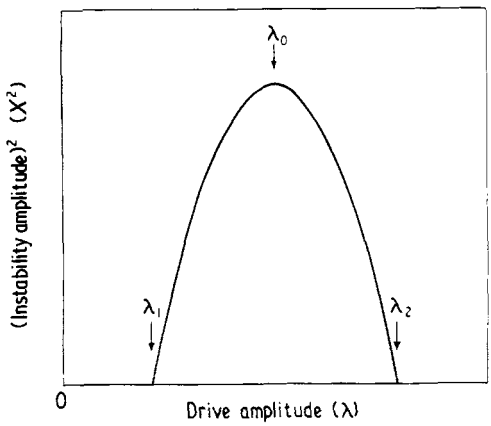

Figure 2. Theoretical predictions of the square of the instability amplitude (X^2) as a function of the drive amplitude λ.

in the region of drive amplitude between λ_1 and λ_2. Further, they have shown that if the drive amplitude is in this range ($\lambda_1 < \lambda < \lambda_2$), that oscillations exist even if the exact resonance condition ($\omega = 2\omega_0$) is not satisfied, and that there is a range of $\Delta\omega(\propto g)$ on either side of $2\omega_0$, where oscillation at ω_0 exists. The relationship between the amplitude and the frequency range can be found from equation (20), and is as indicated in figure 3. The curve (*a*) for λ_0 drive is that corresponding to the maximum amplitude value at exact resonance and curve (*b*) corresponds to a drive value where $\lambda \neq \lambda_0$. It is seen that this phenomenon differs radically from classical linear resonance, which has the appearance shown by the broken curve in figure 3.

2.3. Forcing oscillations near the third harmonic ($\omega = 3\omega_0 + \Delta\omega$)

In this case, equation (14) has the form

$$\frac{d^2x}{d\tau^2} + x = \lambda \sin 3\tau + F\left(x, \frac{dx}{d\tau}\right) \tag{21}$$

where $F(x, dx/d\tau)$ has the value given by equation (15).

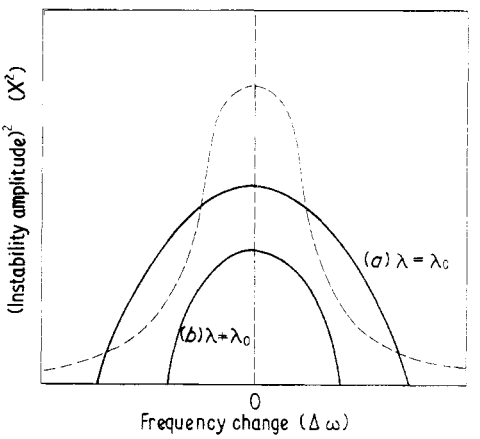

Figure 3. Theoretical prediction of the square of the instability amplitude as a function of the change in frequency $\Delta\omega$ for the case (*a*) $\lambda = \lambda_0$, the optimum value of λ and (*b*) $\lambda \neq \lambda_0$.

In the same way, a trial solution of the following form is adopted:

$$x = a_3 \sin\tau - b_3 \cos\tau - \frac{\lambda}{8}\sin 3\tau$$

$$= X \sin(\tau - \psi) - \frac{\lambda}{8}\sin 3\tau. \tag{22}$$

Upon substitution of the trial form in equation (21), the following relationships must be satisfied for equation (22) to be a solution:

$$a_3\left\{k + \frac{A_3}{4}\left(X^2 + \frac{\lambda^2}{32}\right)\right\} + b_3\left\{\frac{3A_2}{4}\left(X^2 + \frac{\lambda^2}{32}\right) - g\right\}$$

$$= \frac{3a_3 b_3 \lambda A_2}{16} - \frac{(a_3^2 - b_3^2)\lambda A_3}{32} \tag{23}$$

$$b_3\left\{k + \frac{A_3}{4}\left(X^2 + \frac{\lambda^2}{32}\right)\right\} - a_3\left\{\frac{3A_2}{4}\left(X^2 + \frac{\lambda^2}{32}\right) - g\right\}$$

$$= \frac{\lambda A_3 a_3 b_3}{16} + \frac{(a_3^2 - b_3^2)3\lambda A_2}{32}.$$

If $(X^2 + \lambda^2/32) = Y^2$, then equations (23) can be reduced to

$$\left(k + \frac{A_3 Y^2}{4}\right)^2 + \left(\frac{3A_2 Y^2}{4} - g\right)^2 = \left(\frac{\lambda}{32}\right)^2 (9A_2^2 + A_3^2)\left(Y^2 - \frac{\lambda^2}{32}\right). \tag{24}$$

This equation is of the form

$$Y^4 + Y^2 M(\lambda, g) + N(\lambda, g) = 0 \tag{25}$$

and has a solution

$$X^2 = -\frac{\lambda^2}{32} - \frac{1}{2}M(\lambda, g) + \frac{1}{2}\{M^2(\lambda, g) - 4N(\lambda, g)\}^{1/2}. \tag{26}$$

This solution has a similar form to that given by equation (20). Consequently, the variation of oscillation amplitude X at ω_0, with drive amplitude A is anticipated to have a similar variation to that indicated in figure 2. Similarly, the variation of amplitude X with frequency near $3\omega_0$, should show a relationship to that indicated in figure 3.

3. Experimental details

In these experiments, the plasma used was the positive column of a neon arc discharge, similar to that described previously (Keen and Fletcher 1970), and a cross section of the experimental set-up is shown in figure 4. The discharge was formed by applying a DC potential between a mercury pool cathode and a stainless steel anode. The mercury content in the main discharge tube was reduced to a small level by pumping with a combination of mercury diffusion pump close to the pool, and a liquid N_2 cooled cold trap above the pool. The plasma was contained in a glass tube (diameter 5 cm, 180 cm long) by a homogeneous ($\simeq 0{\cdot}5\,\%$) axial magnetic field. This field was variable up to 250 G, but in these experiments was held constant at about 150 G. Neutral neon gas was introduced into the tube near the cathode end, and its pressure could be maintained at a constant value by varying the leakage rate or the pumping rate.

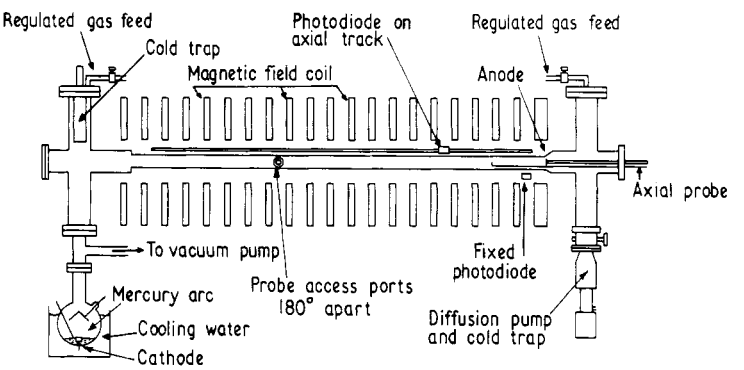

Figure 4. Cross section of experimental apparatus.

Access to the plasma was provided by experimental ports situated along the glass tube, and various interchangeable probes could be inserted at these points. A radially moveable double probe was used to measure the density and electron temperature (T_e) profiles of the plasma. The density profile was found to be approximately parabolic in profile with a peak density of approximately $2{\cdot}5 \times 10^{11}\ \mathrm{cm}^{-3}$ at an arc current of 2 A. The electron temperature T_e was found to be approximately constant in the radial range $r = 0$–2 cm with a value $T_e = 5{\cdot}4 \pm 0{\cdot}2$ eV.

Another probe, inserted from the anode end plate, which could be moved axially and radially was used to observe the instability characteristics, as a function of axial position. Outside the glass tube was an axially moving photodiode. This was used to observe density fluctuations in the plasma, and as it was remote from the plasma did not interfere with any of the plasma parameters.

Initially, the plasma was started with a selfexcited oscillation or instability present. These oscillations were observed with predominantly a single frequency $\omega_0 \simeq 7{\cdot}1$ kHz,

and its radial amplitude, and azimuthal phase variations were consistent with an azimuthal mode number $m = 0$. The axial phase and amplitude measurements showed that the wave was a standing wave in this direction and was four half wavelengths long. The wavelength was approximately 80 cm, and at the frequency of 7·1 kHz this resulted in a phase velocity of $5{\cdot}7 \times 10^5$ cm s^{-1}, compared with the ion sound velocity $c_s = (T_e/M)^{1/2} = 5{\cdot}1 \times 10^5$ cm s^{-1}.

Further experiments were performed to determine the frequency and wavelength variations in both neon and argon plasmas, as the plasma parameters were varied. These variations taken with the facts that the instability frequency was independent of magnetic field and peak density, and that the instability required a critical current for its onset, suggested its identification as an ion sound instability.

After its identification, the oscillation was reduced to its marginal state, such that it was no longer selfexcited. This could be achieved either by decreasing the growth mechanism (by reducing the arc current) or by damping the wave (by increasing neutral pressure and thus the ion–neutral collisions frequency ν). In this case, the latter method was adopted, and the neutral pressure was maintained at about 20 mTorr. The increased pressure had some effect on the wave frequency, and this was found to reduce slightly to approximately 6·8–7·0 kHz, just before the oscillation was quenched.

It was in this marginal state, that the experiments were performed. External signals at frequencies ω_0/m and $m\omega_0$ ($m = 1, 2, 3, \ldots$) were coupled into the plasma from a small magnetic coil wound around the glass plasma tube, which could be moved axially and set at any desired position along the tube. An AC current at the required frequency ω through the coil, produced an AC magnetic field $\tilde{B}_z$ in the plasma. This field had the effect of 'squeezing' and 'relaxing' the plasma, thus modifying the containment pressure p at this position. Consequently, this produced a density oscillation in the plasma, linearly proportional to the current $\tilde{I}$ in the coil (since $\tilde{p} \propto \tilde{n} \propto B_0\tilde{B}_z \propto \tilde{I}$). The effect on the plasma of this driving oscillation at ω was monitored by feeding the output from a floating or ion-biassed probe on to a spectrum analyser. This allowed the instability amplitude at ω_0, as well as the driven amplitude at ω, to be measured simultaneously.

4. Results

4.1. Forcing oscillations at ω_0/m ($m = 1, 2, 3, 4, \ldots$)

Once the neutral pressure had been increased to damp out the instability, experiments were performed with external driving forces at frequencies near ω_0, $\omega_0/2$, $\omega_0/3$, $\omega_0/4$ and $\omega_0/5$. Typical results obtained are shown in figure 5, when the driving force was near the frequency $\omega_0/2$. For a low driving oscillatory current ($I = 1{\cdot}05$ A) the variation of amplitude b with applied frequency ω shown in figure 5(*a*) was obtained. It is seen that a standard symmetrical linear resonance type curve was obtained, as predicted by equation (9). At an increased drive current ($I = 1{\cdot}4$ A), the variation shown in figure 5(*b*) was realized, and it is seen that the resonance curve was asymmetrical with the maximum amplitude value shifted to higher frequencies. When the drive current was increased further ($I = 1{\cdot}75$ A), the variation indicated in figure 5(*c*) was followed. It is seen that as the frequency was increased gradually the path indicated by the open circles was followed, whereas when the frequency was decreased the path marked by the crosses was traversed. Therefore, a hysteresis effect was apparent, as suggested by the theoretical predictions and shown in figure 1(*c*).

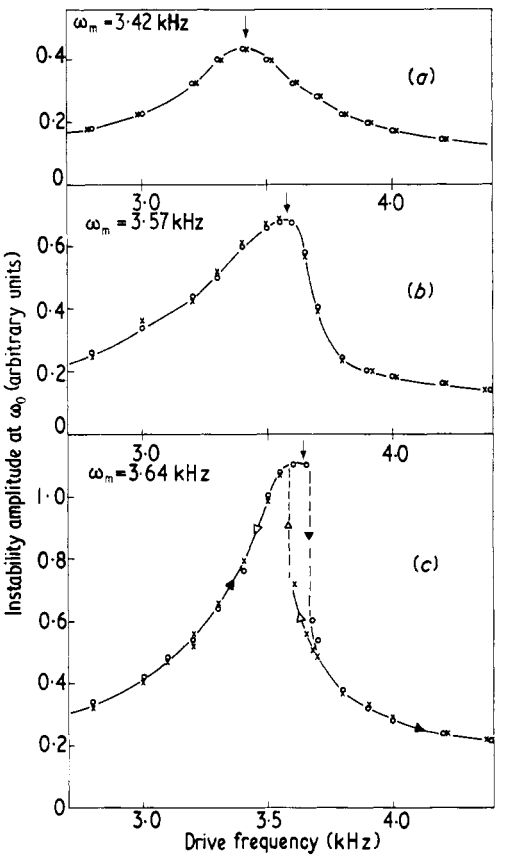

Figure 5. Experimental variation of instability amplitude b as a function of frequency for various drive currents I, (*a*) I = 1·05 A, (*b*) I = 1·4 A and (*c*) I = 1·75 A. The open circles indicate the path followed for increasing frequency and the crosses, that followed for decreasing frequency.

For this drive frequency near $\omega_0/2$, the maximum amplitude b_m was measured as a function of the drive current I. This variation is plotted in figure 6 as b_m against the current squared (I^2). It is seen that a good linear variation ($b_m \propto B^2 \propto I^2$) is apparent, as predicted by equation (12).

Similar variations to those indicated at $\omega \simeq \omega_0/2$ were observed when forcing oscillations near $\omega \simeq \omega_0$ were used. When forcing at frequencies near $\omega_0/3$, $\omega_0/4$ and $\omega_0/5$, insufficient oscillatory current flowed in the driving coil in order to obtain asymmetrical resonance and hysteresis effects. However, the instability could be induced at ω_0 when driving at these frequencies, and the amplitude b at ω_0 as a function of frequency between $\omega_0/5$ and $\omega_0/2$ for a constant drive current (I = 1·4 A), is plotted in figure 7.

4.2. Forcing oscillations near $2\omega_0$

With the frequency set at $\omega = 2\omega_0$ ($\omega_0 \simeq$ 6·85 kHz), the drive current I through the coil at this frequency was increased gradually, and the instability level at ω_0 was

monitored. At a current $I \simeq 0{\cdot}8$ A, the instability at ω_0 appeared above the background noise, and as the current was increased further, this amplitude increased until at $I = 1{\cdot}3$ A the instability reached a maximum value. Further increase in current reduced the level and the instability disappeared for currents greater than $I = 1{\cdot}8$ A, even though values up to 4 A were attained. The variation of amplitude squared (X^2) at ω_0, as a function of the drive current I at $2\omega_0$ is shown in figure 8.

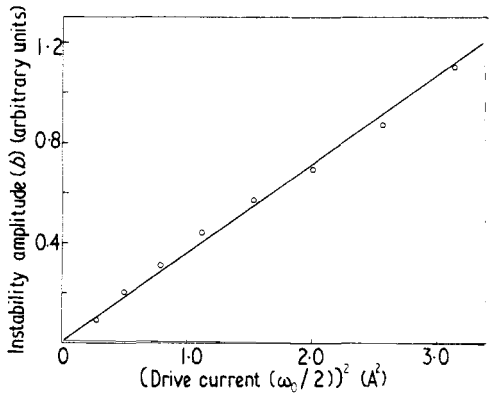

Figure 6. Maximum instability amplitude b_m as a function of the square of the drive current (I^2).

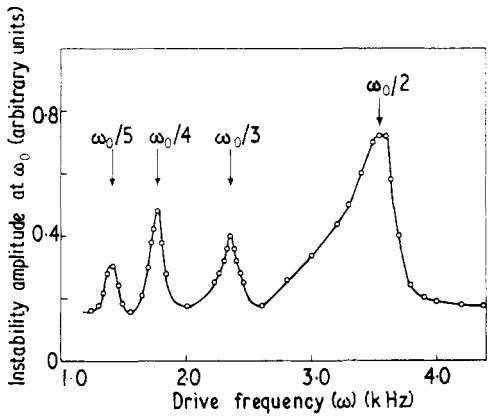

Figure 7. Instability amplitude b as a function of drive frequency ω.

At the optimum current drive ($I \simeq 1{\cdot}3$ A) the amplitude X was measured as the frequency was varied close to $2\omega_0$. Starting at a value $\omega \simeq 12$ kHz, the frequency was increased gradually, until the instability appeared above the noise level at about $\omega \simeq 12{\cdot}5$ kHz. As the frequency was increased further the amplitude X increased and reached a maximum value at $\omega = 2\omega_0$, then decreased and disappeared at $\omega = 14{\cdot}9$ kHz. This is shown in figure 9 where the square of the instability amplitude (X^2) is plotted as a function of frequency variation.

The observed variations in both figures 8 and 9 are similar to the theoretical predictions which were shown in figures 2 and 3 respectively.

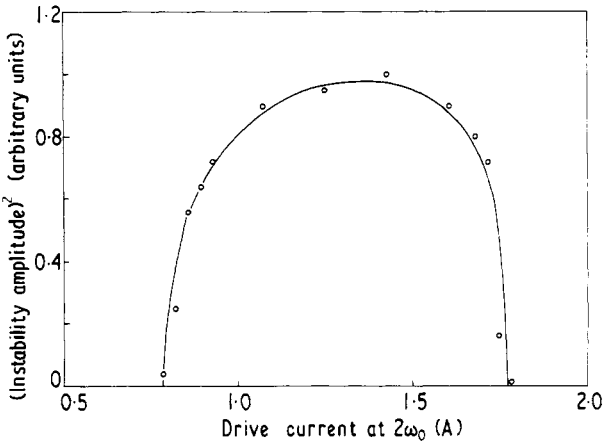

Figure 8. The square of the instability amplitude X_2^2 as a function of drive current for a drive frequency $\omega = 2\omega_0$.

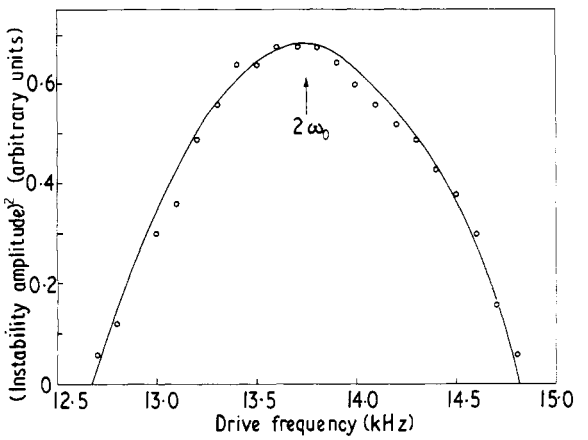

Figure 9. The square of the instability amplitude X_2^2 as a function of frequency ω near $\omega \simeq 2\omega_0$ at constant drive current $I = 1{\cdot}3$ A.

4.3. Forcing oscillations near $3\omega_0$

Similar experiments were performed with the driving oscillations ω near $3\omega_0$. In this case, when the system was driven at $\omega = 3\omega_0$ and the current increased, the instability amplitude X increased above noise at $I \simeq 1{\cdot}2$ A, and reached a maximum at $I = 3{\cdot}0$ A. However, the driving current could only be increased to $I = 4$ A, and thus, the instability could not be made to disappear for higher drive currents, although it did begin to decrease above $I = 3$ A. This variation of X^2 against drive current I is shown in figure 10.

The variation of X^2 against frequency (near $3\omega_0$) is shown in figure 11, performed at two current values $I = 1{\cdot}4$ A, and at the optimum value $I_m = 3{\cdot}0$ A. Again, the variation is similar to that predicted by theory and shown in figures 2 and 3.

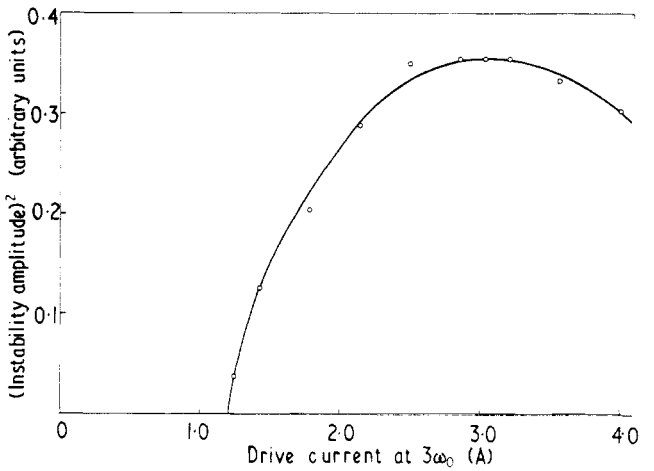

Figure 10. The square of the instability amplitude X^2 as a function of drive current at $\omega = 3\omega_0$.

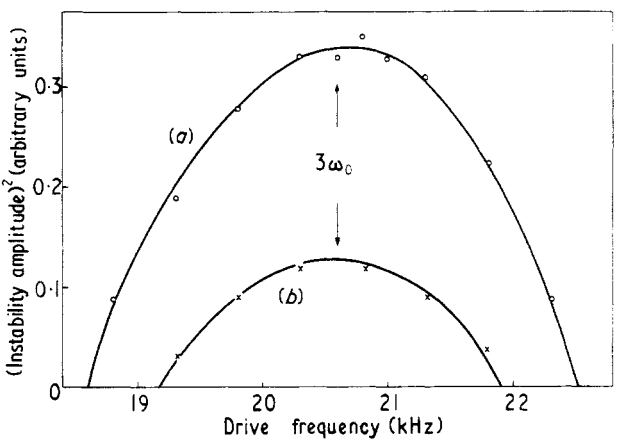

Figure 11. The square of the instability amplitude X^2 as a function of the frequency ω, near $\omega \simeq 3\omega_0$, at a constant drive of (*a*) $I = 3{\cdot}0$ A, and (*b*) $I = 1{\cdot}4$ A.

5. Discussion and conclusions

In § 2, it was shown that the perturbed density amplitude n_1 of the ion sound wave could be described by an equation similar to the classical Van der Pol (1922) oscillator, but including anharmonic terms. Further, it was shown that if an external driving force of frequency ω was applied to the system that this marginal instability behaved in a different fashion depending upon whether the applied frequency was near to a harmonic frequency, or near the fundamental frequency or a subharmonic frequency.

For drive frequencies ω close to the fundamental or a subharmonic $\omega = \omega_0/m$ ($m = 1, 2, 3, \ldots$) theory predicts that the amplitude of the instability at ω_0 is given by equation (9). At small driving amplitudes, this equation reduces to a standard symmetrical forced resonance equation, which has a maximum at $\omega \simeq \omega_0$ and a shape indicated in figure 1(*a*) as the frequency is varied. At higher drives the shape changes and the curve becomes asymmetrical with the maximum amplitude shifted to higher

frequency values (figure 1(*b*)). At even higher drive amplitudes, the classical 'jump' phenomenon is indicated and a hysteresis effect occurs, as shown in figure 1(*c*). A comparison between the experimentally measured phenomena and these theoretical predictions shows them to be in good agreement.

For drive frequencies close to the second harmonic ($\omega \simeq 2\omega_0$) or the third harmonic frequency ($\omega = 3\omega_0$), theory predicts that the system should behave in a manner similar to a parametric oscillator (Mandelstam and Papelexi 1932). The amplitude of the instability in each case should be given by equations (19) and (25) respectively. The predicted shape of the amplitude variation as a function of frequency is radically different from the classical linear resonance curve which is shown in figure 3 for comparison with this case. Also, theory predicts that as the drive amplitude at $\omega(\simeq 2\omega_0$ or $3\omega_0)$ is increased from zero, the instability amplitude at ω_0 does not appear above the noise level until a certain drive level λ is attained. Thus, further increasing the drive λ increases the instability amplitude until a maximum level is reached at λ_0. Subsequent increase of λ only reduces the amplitude level and finally goes to zero at λ_2. This variation has been observed when forcing at approximately $2\omega_0$, but experimental limits prevented the increase of the drive level at $3\omega_0$ from observing the upper point at λ_2. However, a comparison between the theoretical predictions and the experimental measurements in the regime shows remarkably good qualitative agreement.

Consequently, it has been shown that good qualitative agreement is obtained between theory and experiment for nonlinear behaviour of the marginal ion sound instability in a plasma. In principle, this suggests a method for obtaining values for the particular nonlinear saturation coefficients β and γ, and the linear growth-rate parameter $\alpha/2$ relevant to a particular instability in a plasma.

References

Dupree T H 1968 *Phys. Fluids* **11** 2680–94.
Hendel H W, Chu T H and Politzer P A 1968 *Phys. Fluids* **11** 2426–39.
Hsuan H C S 1968 *Phys. Rev.* **172** 137–45.
Keen B E and Fletcher W H W 1969 *Phys. Rev. Lett.* **23** 760–3.
—— 1970 *J. Phys.* D: *Appl. Phys.* **3** 1868–85.
Mandelstam L and Papalexi N 1932 *Z. Phys.* **73** 223–48.
Minorsky N 1962 *Nonlinear Oscillations* (Princeton, NJ: Van Nostrand).
Stix T H 1969 *Phys. Fluids* **12** 627–39.
Van der Pol B 1922 *Phil. Mag.* **43** 700–13.